Effect of form errors on the positioning precision of over-constrained systems

Denis Teissandier [a], Yann Ledoux [a], Santiago Arroyave-Tobon [c], Vincent Delos [b], Jean Marc Linares (1)[c,*]

[a] Univ. Bordeaux, I2M, UMR 5295, F-33400 Talence, France
[b] CNRS, I2M, UMR 5295, F-33400 Talence, France
[c] Aix Marseille Univ., CNRS, ISM, Marseille, France

ARTICLE INFO

ABSTRACT

This paper analyses the influence of form deviations on over-constrained mechanical systems. A mechanical clamp was equipped with LVDT sensors to measure relative displacements between its two parts to derive their relative position. Each part was measured using CMM filtering its form deviations. Part feature variations (position, orientation and dimension) and assembly clearances were aggregated on a set of 6d linear constraints. From the measured local displacements another polytope is derived. These two polytopes are compared to quantify the influence of form error on the geometrical behaviour of the assembly. To do this evaluation new metrics are presented and discussed.

© 2019 Published by Elsevier Ltd on behalf of CIRP.

1. Introduction

The objective of a tolerance analysis is to aggregate the geometric error variations of the constitutive parts of a mechanical system in order to check the functional requirements. Such an analysis process is based on: a model of geometric error variations, a set of relations between them derived from the topological structure of the mechanical system and numerical tools to simulate its geometrical behavior. This tolerance analysis can be done according to worst case or statistical approaches [1]. The major question is how to select the suited values of geometrical product specifications in order to control the geometric error variations (form, orientation, position and dimension) to guarantee the expected product quality. To simplify the tolerance analysis, some assumptions are usually made, among which form errors are neglected and mechanism parts are considered as infinitely rigid bodies. These assumptions could lead to inaccuracies in the computation results as shown by Ref. [2]. Only a few research works, summarized in Ref. [3], address the effect of form error variations on the geometrical behavior of an assembly. This is a key point in mechanism analysis that should be quantified. Some works are based on experimental devices to compare the simulated and the real behaviors of the assembly. However, these works were dedicated to analyze, experimentally, isostatic assemblies.

In this work, a practical case study is used to demonstrate the influence of form errors in the positioning precision on over-constrained mechanical systems. Error metrics are proposed to quantify that. In the context of Industry 4.0, these metrics are computed using a digital twin of the mechanical system. Their uses in production control are discussed in the manufacturing field. In a first part of this paper, a geometrical model for over constrained mechanisms is set up assuming no error from variations. An example of a mechanical clamp with 2 parts and their several parallel joints is treated. In the second part, based on rigid body restrictions, the influence of the form error variations on the relative position between two parts is evaluated. This evaluation is based on the comparison of the calculated and the measured displacements due to geometrical errors. To do this evaluation four new metrics are presented and discussed.

2. Materials and methods

The parts were modeled as infinitely rigid bodies. The displacement restrictions induced by the non-interpenetration conditions between two surfaces potentially in contact are formalized by a set of linear constraints [4–6]. Each set of contact constraints is represented by a polyhedron shown in the next section [7].

2.1. Geometrical model for over-constrained systems

Let us consider a contact restriction between surfaces 1_j (surface j of part 1) and 2_j (surface j of part 2), see Fig. 1. The general definition of the contact restriction is given by (1). This definition is applied to a set of N_k points (with $1 \leq k \leq k$max and $k$max is the number of facets for the discretization of each contact surface). At each point, the contact restriction is applied along the normal vector $\mathbf{n}_k$ where d_k is the distance between 1_j and 2_j. The
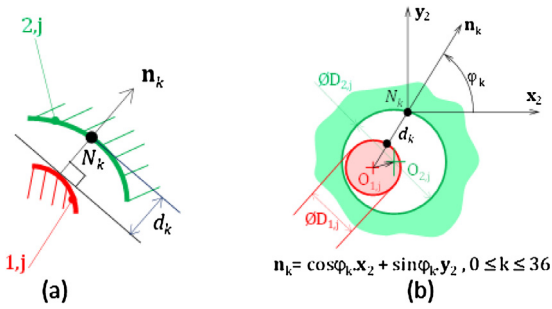
Fig. 1. Local (a) and global (b) contact restrictions.

intersection of this set of restrictions defines the polyhedron Pj.

$$P_j = \bigcap_k (\boldsymbol{t}_{Nk_1,j/2,j}).\boldsymbol{n_k} \le d_k \Longleftrightarrow$$
$$P_j = \bigcap_k (\boldsymbol{t}_{o_1,j/2,j} + \boldsymbol{N_k O} \times \boldsymbol{r}_{1,j/2,j}).\boldsymbol{n_k} \le d_k \qquad (1)$$

P_j is a polyhedron of dimension 6 since each local contact restriction is a half-space $\overline{H_k^-}$ in the deviation space of dimension 6 [7]. The 6 parameters ($R_x, R_y, R_z, T_x, T_y, T_z$) are coming from the components of $r_{1,j/2,j}$ (rotation vector) and $\boldsymbol{t}_{O\,1,j/2,1}$ (translation vector expressed at point O). The point O is any point assumed to be rigidly linked to the set of points N_k. Let us consider a mechanical assembly composed of two parts: part 1 and part 2, in multiple relations by several contacts in parallel between surface 1,j and 2,j ($1 \le j \le j$max): see Fig. 2. A datum R_1 is associated to the surfaces 1,j of part 1 by measurements. Following the same method, a datum R_2 is associated to the surfaces 2,j of part 2. The determination of the local distances d_k from (1) takes into account the location deviations of 1,j with respect to R_1 ($\boldsymbol{d}_{1,j/R1}$) and 2,j with respect to R_2 ($\boldsymbol{d}_{2,j/R1}$). The relative position between R_1 and R_2 is defined by P_c. P_c is the intersection of the n polyhedron P_j ($1 \le j \le j$max; where $j$max is the number of contact surfaces). If the contacts between parts 1 and 2 suppress the 6 degrees of freedom, P_c is a polytope (i.e. a bounded polyhedron). Then the vertices of P_c define the extremal values of the parameters ($R_x, R_y, R_z, T_x, T_y, T_z$) in a deviation space. P_c is the result of the intersection between ($j$max × $k$max) local restrictions (i.e. half-spaces of dimension 6). Finally, we will use the general expression (2), commonly named H-description, to define the polytope P_c. According to the Minkowski–Weyl theorem [8], an equivalent definition (3) can be used for P_c where v_{ci} are the vertices of P_c.

$$P_c = \bigcap_j P_j = \bigcap_u \overline{H_u^-} \text{ with} : 1 \le u \le j\text{max} \times k\text{max} \qquad (2)$$

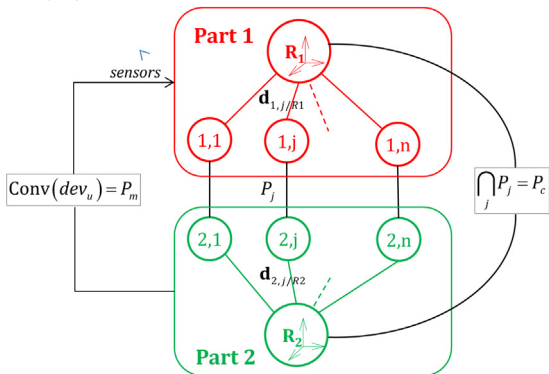$$P_c = Conv(v_{ci}) \qquad (3)$$

Fig. 2. Contact restrictions at the assembly level.

The definition (3) is commonly named the V-description of P_c, where P_c is defined by the convex hull of its vertices v_{ci}. We use this theorem in order to directly measure the relative position between parts 1 and 2 by a measured polytope P_m. A mechanical system was instrumented by sensors which measures a finite number of relative positions between parts. Each position corresponds to a set of parameters defined by a point dev_u in the deviation space.

Finally, P_m can be estimated by the convex hull of points dev_u according to (4) where $u$max is the number of measures to generate the points dev_u.

$$P_m = \text{Conv}(dev_u) \quad 1 \le u \le u\text{max} \qquad (4)$$

2.2. Experimental protocol

Our aim is to evaluate the influence of the form error variations on the relative position between two parts in contact in the case of an over constrained assembly. This evaluation is based on the comparison between the calculated polytope P_c and the measured polytope P_m. The surfaces 1,j and 2,j are modeled by substitute surfaces through the measurement process, in order to eliminate the form deviations by least square best-fit method (i.e. gaussian filters). So, the polytope P_c is the aggregation of orientation, position and dimension variations. The convex hull of points (dev_u) derives from direct measurements of the relative position between parts. The polytope P_m is then the aggregation of all the possible sources of geometrical variations of surfaces 1,j and 2,j (i.e. orientation, position, dimension and then form errors).

The study is carried out on a mechanical system inspired by a clamp (Fig. 3a and b). The constitutive parts 1 and 2 are in multiple contacts by three couples of pin 1,j – hole 2,j ($1 \le j \le 3$) with a nominal diameter equal to Ø10. These couples are evenly distributed on a nominal circle (Ø80) (Fig. 3c). Two additional datums 1,4 and 2,4 respectively on part 1 and part 2, are nominally located on the center of this circle. These respective center holes $O_{1,4}$ and $O_{2,4}$ with a fixed square on part 1 are used to measure the relative position between datum R_1 and datum R_2 respectively linked to parts 1 and 2. We define contact restrictions assuming the contact zones between pins and holes lie in the same plane (i.e. the common plane between parts). As a consequence, the relative position between R_1 and R_2 is defined by a small rotation along a normal to the common plane and two orthogonal translations in this plane. The polytopes P_c and P_m are both 3d polytopes. The origin of datum R_1 is defined by $O_{1,1}$ and one axis by the square. The origin of datum R_2 is defined by $O_{2,1}$ and one axis by a line ($O_{2,1}$, $O_{2,4}$).
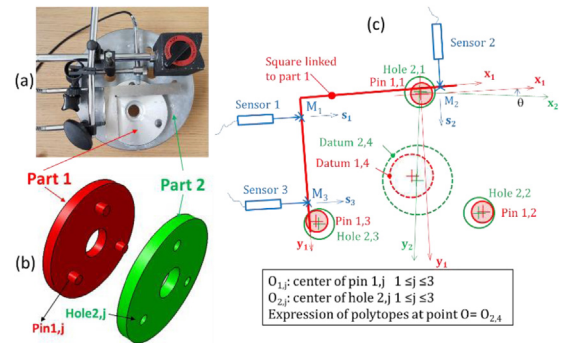

Fig. 3. Experimental device (a); CAD part (b); geometric setting of the clamp (c).

The five steps of the analysis protocol are depicted in Fig. 4.

First, part 1 is measured to estimate the location of surfaces 1,j in R_1 and their diameters $ØD_{1,j}$ (step 1). By analogy, surfaces 2,j in R_2 and their diameters $ØD_{2,j}$ are estimated on the part 2. Each surface is measured by 8 points evenly distributed with a CMM machine (Renishaw® TP20, measurement uncertainty: 7 μm in volume). Although they are not used in the computation of polytope P_c, the form deviations of each contact surface are also evaluated. In step 2, part 1 is assembled on part 2 and fixed in an arbitrary location such as their common planes are in contact. Then, in step 3, the square and the hole 1,4 are measured in R_2 and the LVDT sensors are initialized in this configuration. This is a major step in the best-fit of the origins of polytopes of P_c and P_m. In step 4, an operator manually moved part 1 with respect to part 2 reaching as many extremal positions as possible. The motions between parts are measured by the three LVDT sensors (DP5 probes of Solartron Metrology® with accuracy of 0.5 μm). Finally, all the data are saved to be used for the computation of polytopes P_c and P_m (step 5).
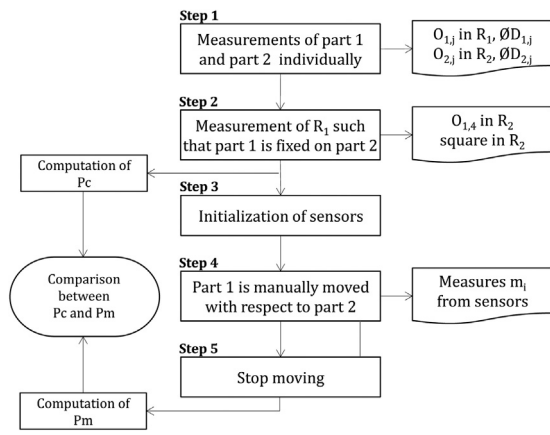
Fig. 4. Experimental protocol.

2.3. Computed polytope Pc

The contact restrictions between pin 1_j and hole 2_j derive from definition (1), and P_j can be expressed as (5).

$$P_j = \bigcap_k (t_{O_1 j/2 j} + N_k O \times r_{1j/2j}) . n_k \leq d_k$$

$$with\ d_k = \left(\frac{D_{2,j} - D_{1,j}}{2}\right) + O_{1j} O_{2j} \cdot n_k \tag{5}$$

The couples $N_k,\ \mathbf{n}_k$ are deduced from a mesh built on the CAD model of the clamp. This couple and the point O control the normal of each half-space $\overline{H_k^-}$. An operand P_j is generated with $k$max = 36 such that the maximal deviation between the mesh and the surfaces of pin 1_j and hole 2_j is less than 1 μm [7]. The other parameters to compute a local distance d_k are coming from the diameters and the location deviations of pin 1_j and hole 2_j. Their values derive from the measurements performed in steps 1 and 2 of the synoptic (see Fig. 4). Least square filtering is used to remove the form deviations to others for pins 1_j and holes 2_j. From (2) the polytope P_c can be computed as shown in Fig. 5.
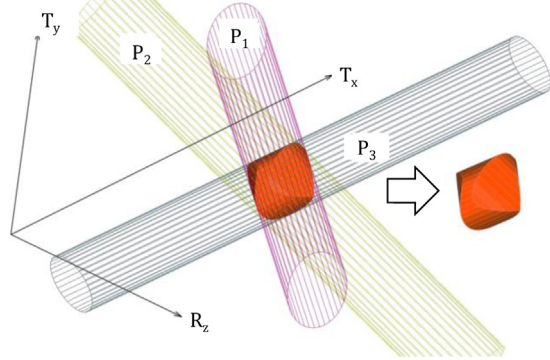

Fig. 5. Polytope $P_c = P_1 \cap P_2 \cap P_3$.

2.4. Measured polytope P_m

From local measures of the sensors, we obtain a set of relations using Eq. (6). These relations can be expressed at a common point O assumed to be rigidly linked with the points M_i. Then the parameters R_z, T_x and T_y can be determined from (6) with (7) and (8) by (9).

$$\{t_{Mi_R 1/R2} . s_i = m_i\}\, 1 \leq i \leq 3 \tag{6}$$

$$t_{Mi_R 1/R2} = t_{O_R 1/R2} + r_{R1/R2} \times M_i O \tag{7}$$

$$s_i = (s_{ix}, s_{iy}, 0) \quad OM_i = (OM_{ix}, OM_{iy}, 0)$$

$$r_{R1/R2} = (0, 0, R_z) \quad t_{O_R 1/R2} = (T_x, T_y, 0) \tag{8}$$

$$\{(-s_{ix}.OM_{iy} + s_{iy}.OM_{ix})R_z + s_{ix}.T_x + s_{iy}.T_y = m_i\}\, 1 \leq i \leq 3 \tag{9}$$

Finally, from $u$max records of triplets m_i we can deduce a cloud of points dev_u in a deviation space (R_z, T_x, T_y).

3. Results and discussions

3.1. Measured polytope P_m

Fig. 6a gives an example with 2000 records of triplets m_i. Fig. 6b shows the polytope P_m resulting from the convex hull of 2000 points. The vertices of P_m are the extremal displacements between parts 1 and 2 reached by the manual operation. The point density on the boundary of P_m is very heterogeneous.
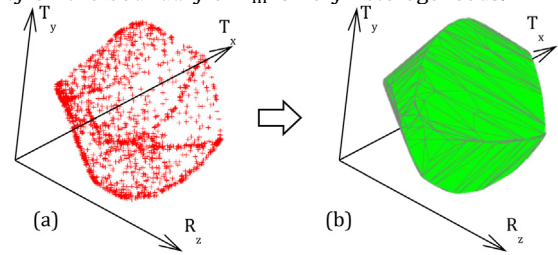

Fig. 6. Cloud of 2000 points (a) and its convex hull P_m (b).

3.2. Computed polytope P_c

The results of the CMM measurement of parts 1 and 2 are displayed in Table 1. The vertices of P_c result from the intersections of its half-spaces initially generated on the nodes of a regular mesh, see Figs. 5 and 7.

3.3. Comparison between polytopes P_m and P_c

The difference between the shape of polytopes P_c and P_m is due to the form deviations. Based on Eq. (5), the distance d_{k*} between a pin 1_j and a hole 2_j is redefined by (10).

$$d_{k*} = d_k + fv_k \tag{10}$$

The parameter fv_k is the accumulation of form error deviation of a pin 1_j with respect to a hole 2_j at a node N_k along the normal $\mathbf{n}_k$, see Fig. 1. It was filtered by the best-fit process after the CMM measurement of parts 1 and 2 and it is not taken into account in (5). In consequence, form error variations generate a translation fv_k of the half-space $\overline{H_k^-}$ along its normal. In general, the parameters fv_k have an influence on the boundary of the intersection of these half-spaces. Each vertex of a polytope defines an extremal position between the parts 1 and 2 and is created by a minimum of 3 concurrent hyperplanes in dimension 3. These hyperplanes are the boundaries of the half-spaces deriving from some points N_k which define the contact zone between the parts 1 and 2. The relation between the half-spaces and the vertices ensures the complete traceability between nodes $N_k,\ \mathbf{n}_k$ and the extremal positions extracted from its faces [7]. The comparison between polytopes P_m and P_c cannot be done based on properties of their

Table 1
Measurement results of individual parts 1 and 2 in R_2 in mm.

Surface	1,1	1,2	1,3	2,1	2,2	2,3
Form dev	0.014	0.011	0.012	0.007	0.009	0.007
Diameter	10.004	10.008	10.006	10.554	10.558	10.557
Loc x Loc y	−0.273 39.973	34.904 20.070	−34.422 20.056	0.000 40.000	34.663 19.995	−34.619 19.995
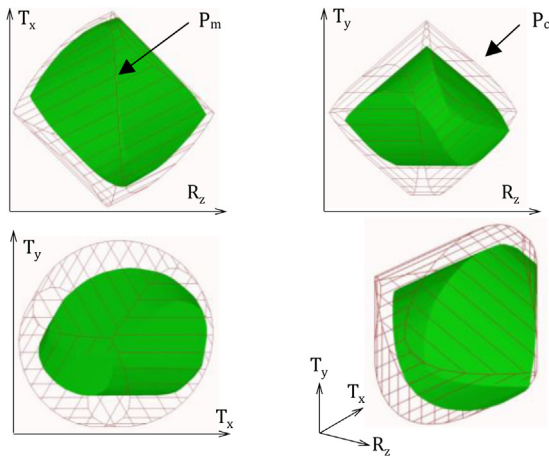
Fig. 7. Projections of polytopes P_c and P_m in canonical views.

Fig. 8. Hausdorff distances between tessellation of P_m with respect to the boundary of P_c.

lattices. Therefore, the direct estimation of the values fv_k is not possible. In response to this, new geometrical metrics are proposed to compare P_m and P_c such as the bounding boxes, the mass centers, the volumes and the Hausdorff distances [9]. The bounding box of P_m is included inside the bounding box of P_c. According to the parameters (R_z,T_x,T_y), the ratios of the three extends of the bounding boxes are 88%, 87% and 67%, see Table 2. If we want to limit the global motions of one part compare to the other one, this bounding box computation is a useful quantification. It is also, a well indication of the positioning precision of the parts (small volume meaning a small motion).

Table 2
Bounding boxes of polytopes.

Bounding box	R_z (10^{-3} rad)	T_x (mm)	T_y (mm)
P_c	[−7.321; 6,384]	[−0.510; 0.023]	[−0.302; 0.207]
P_m	[−6.190; 5.860]	[−0.456; 0.007]	[−0.217; 0.133]
Ratio P_m/P_c	88%	87%	67%

These results do not integrate the correlations between the parameters (R_z,T_x,T_y).

Assuming that the relative position of parts is randomly distributed in the polytope, the vector **GcGm** then gives the average of the relative location between datum R_1 and R_2 in terms of (R_z,T_x,T_y) in the 3d deviation space, see Table 2. The magnitude and the direction of this vector are strongly correlated to the distribution of fv_k on the contact surfaces (Table 3).

Table 3
Mass centres of polytopes.

Mass center	R_z (10^{-3} rad)	T_x (mm)	T_y (mm)
G_c (P_c)	−0.468	−0.247	−0.056
G_m (P_m)	−0.165	−0.211	−0.065
G_cG_m	0.303	0.026	−0.009

Furthermore, the polytope P_m is not included inside the polytope P_c but the volume of $P_c \cap P_m$ is very closed to the volume of P_m, see Table 4. These volumes indicate the inclusion rate and traduce if the polytope P_c increase or not the extremal displacements of P_m. These two-last metrics (G_cG_m and volumes) can help a designer to validate a design choice in a preliminary design stage.

Table 4
Volumes of polytopes in 10^{-3} mm^2.rad.

	P_c	P_m	$P_c \cap P_m$
Volume	46.04	25.58	25.46

Finally, the deviations from the tessellated boundary of P_m with respect to the boundary of P_c can be deduced by a set of distances, see Fig. 8. Each distance is the Hausdorff distance between a point from the boundary of P_m and P_c. Each signed distance indicates if
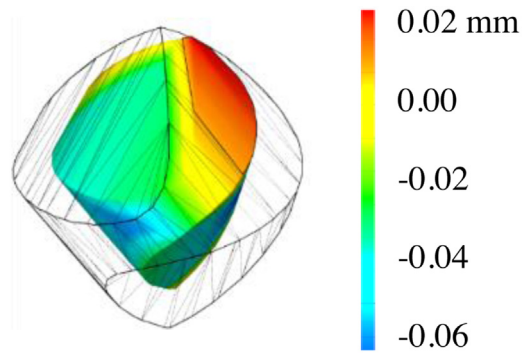
the form deviation must be added or subtracted along a given direction in the neighborhood of an extremal position between the parts 1 and 2. These distances and their directions can lead to detect what half-space $\overline{H_k^-}$ are on the boundary of P_m. Thus, it is possible to investigate about the evolution of the contact zones with and without form error variations in a geometrical model. This diagnosis can lead to detect precisely where are the influent zones on the relative position between parts 1 and 2. Furthermore, this diagnosis can be useful to analyze the load transfer between the parts in order to predict the mechanical behavior of the assembly. These new metrics were integrated in the open source software (i2m.u-bordeaux.fr/politopix).

4. Conclusion

A complete analysis protocol to evaluate the influence of the form error variations on the relative position between parts of an over constrained assembly was presented. This study proposes new metrics to detect and localize assembly interferences induced by form deviations. Moreover, it brings to the fore the influence of form errors in the positioning precision. The four proposed metrics were: Bounding boxes, Mass centers, Volumes of polytopes and Hausdorff distances. In future, the metric uncertainties will be evaluated in order to take into account the effect of assumptions (rigid body, small screw displacement, surface discretization, . . .) and measure uncertainties. These metrics can help designers to take decisions in geometrical product specification. Additionally, they could be used in Industry 4.0, for example in smart part pairing, for choosing the constitutive parts that warrantee an assembly with no interference. This could be done, in real time in the production chain, by digital twin assembly simulation. The knowledge of the assembly interference localization opens the way to automatic processes to repair high added value parts.

References

[1] Cao Y, Liu T, Yang J (2018) A Comprehensive Re view of Tolerance Analysis Models. *The International Journal of Advanced Manufacturing Technology* 97(–8):3055–3085.
[2] Grandjean J, Ledoux Y, Samper S (2013) On the Role of Form Defects in Assemblies Subject to Local Deformations and Mechanical Loads. *The International Journal of Advanced Manufacturing Technology* 65(9):1769–1778.
[3] Xingyu Y, Alex B (2019) Review and Comparison of Form Error Simulation Methods for Computer-Aided Tolerancing. *ASME Journal of Computing and Information Science in Engineering* 19:1–16. 010802.
[4] Fleming A (1988) Geometric Relationships Between Toleranced Features. *Artificial Intelligence* 37:403–412.
[5] Giordano M, Duret D, Tichadou S, Arrieux R (1992) Clearance Space in Volumic Dimensioning. *CIRP Annals — Manufacturing Technology* 41(1):565–568.
[6] Davidson J, Mujezinovic A, Shah J (2002) A New Mathematical Model for Geometric Tolerances as Applied to Round Faces. *ASME Journal of Mechanical Design* 124:609–622.
[7] Arroyave Tobon S, Teissandier D, Delos V (2017) Tolerance analysis with polytopes in HV-description. *ASME Journal of Computing and Information Science in Engineering* 17:1–9. 041011.
[8] Ziegler GM (2012) *Lectures on Polytopes*, vol. 152. Springer Science & Business Media.
[9] Ushakov VN, Lebedev PD, Tarasyev AM, Ushakov AV (2015) Optimization of the Hausdorff distance between convex polyhedrons in R3. *IFAC-PapersOnLine* 48 (25):197–201.